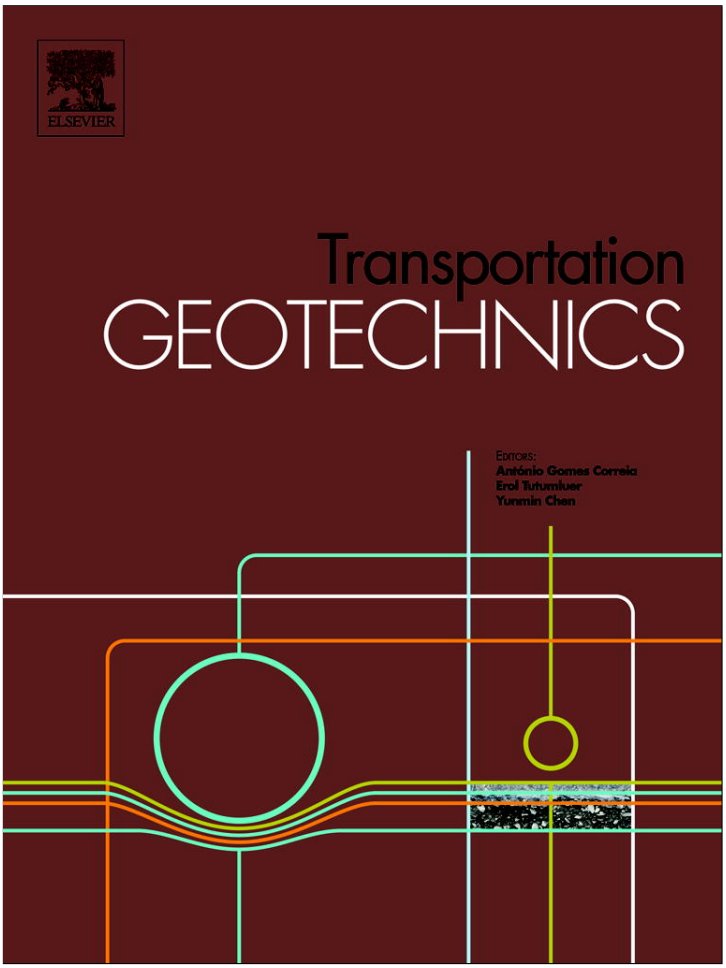

Transportation Geotechnics 1 (2014) 63–73

Contents lists available at ScienceDirect

Transportation Geotechnics

journal homepage: www.elsevier.com/locate/trgeo

Load transfer of hollow Fiber-Reinforced Polymer (FRP) piles in soft clay

J. Giraldo [a], M.T. Rayhani [b,*]

[a] Carleton University, Civil and Environmental Engineering, Ottawa, Ontario, Canada
[b] Dept. of Civil and Environmental Engineering, Carleton University, Ottawa K1S 5B6, Canada

ARTICLE INFO

Article history:
Received 3 February 2014
Revised 6 March 2014
Accepted 13 March 2014
Available online 20 March 2014

Keywords:
Pile
Interface
Load test
Shear strength
FRP
Composite

ABSTRACT

This paper describes results of a series of small scale static axial and lateral pile load tests carried out on model Fiber Reinforced Polymer (FRP) piles and steel piles. The goal of this study was to establish the geotechnical frictional performance of FRP piles in clayey soils compared to hollow steel piles. Hollow FRP piles were manufactured using both carbon and glass fibers with different fiber orientations. Pile load testing was carried out in large undisturbed clay samples using small scale piles of 55 mm in diameter by 700 mm in length. The axial bearing capacity of FRP piles were shown to be 5-40% higher compared to the steel pile. Under lateral loading, the FRP piles presented increased deflections compared to the steel counterpart. Based on the results presented here, FRP piles present suitable characteristics to act as a load bearing member based on axial geotechnical capacity. The structural integrity and excessive deflections need further investigation.

Introduction

Pile foundations are typically constructed using three types of materials or combinations thereof: steel, concrete and wood. However, the use of these materials faces several challenges when installed in harsh environments such as waterfront areas or contaminated and harsh soil conditions. Steel and concrete are subject to corrosion and degradation, leading to significant reduction of pile cross-sectional area and therefore impacting the pile's performance and structural integrity, and drastically reducing service life. In order to address these adverse effects, researchers have been exploring the use of alternate materials such as glass or carbon fibers and plastic composites as piling alternatives. Development and use in other industries has driven the price of production down to an attractive price point and produced a commercially viable technology. In recent decades researchers and industry partners have strived to develop and introduce the use of FRP piles for waterfront and harbour fender pile applications. Iskander and Hassan (1988) highlighted the predominant use of Fiber Reinforced Polymer (FRP) piles for fendering and light load bearing applications in harbours and piers. They cited the lack of an established track record, the lack of design guidelines and high initial material costs as reasons for the limited use in other piling applications. Typical FRP piles are fabricated using either a high density polyethylene (HDPE) matrix reinforced with steel or glass fiber, or fabricated from carbon or glass fiber in the form of hollow shells (Guades et al., 2012). Carbon or glass FRP hollow shells are also in-filled with concrete, in which case the outside fiber shell acts as the pile reinforcement and protect the concrete. In addition the confinement enhances the structural strength and stiffness of the pile (Fam and RizKalla, 2001a,b).

FRP pile performance and soil–pile interface behaviour has been poorly characterized due to the lack of

* Corresponding author. Tel.: +1 61352026008890.
E-mail address: mohammad.rayhani@carleton.ca (M.T. Rayhani).

http://dx.doi.org/10.1016/j.trgeo.2014.03.002
2214-3912/

widespread use of the material. Researchers such as O'Rourke et al. (1990) carried out direct shear box interface characterization tests using sands and HDPE geotextiles where it was found that the interface shear strength increased with sand density and decreased with surface roughness. Frost and Han (1999) conducted a series of interface characterization tests involving FRP interfaces and sand in which they identified various parameters that affected interface shear strength including normal stress levels, soil particle angularity and particularly interface surface roughness. Further studies carried out by Pando et al. (2002) confirmed that interface surface roughness, particle shape and angularity play significant roles in the shear strength behaviour of the soil–pile interface.

Pile drivability and installation is crucial when assessing the use of FRP piles as deep foundation. Due to inherent material properties such as lower stiffness, impedance and density leading to higher damping, hollow FRP piles have a lower driving performance compared to traditional piles. Iskander et al. (2001) carried out a numerical analysis focusing on the drivability of FRP composite piles in which they identified that material properties such as specific weight and elastic modulus played critical roles in driving performance, whilst for stiffer piles, driving behaviour depended mostly on the soil properties. Ashford and Jakrapiyanun (2001) analysed the dynamic pile driving response of a series of steel, concrete and FRP piles. Their results indicate that FRP piles perform comparatively well compared to traditional piles, however lower material impedance limited the ultimate capacity achieved at driving refusal. Mirmiran et al. (2000) analysed the dynamic response to driving for a series of concrete, concrete infilled and hollow FRP piles, and concluded that concrete in-filled FRP piles performed on par with conventional concrete piles, however hollow FRP shells were at risk of compression failure and could support driving stresses of up to 50% at driving refusal compared to the concrete pile.

Pando et al. (2006) carried out a large scale pile load test investigating the performance of FRP piles as the supporting structure for a highway overpass in Virginia. They compared driven pre-cast concrete piles to concrete in-filled FRP piles. Axial pile load tests showed that the FRP piles performed comparably to the concrete pile. Han and Frost (2000) highlighted the importance of non-linearity effects of the flexural stiffness of FRP piles and increased deflections caused by shear deformations due to high elastic modulus to shear modulus ratios. Sakr et al. (2004) compared the performance of driven FRP piles to steel piles in sand and found that FRP piles performed favorably with respect to axial compression compared to steel piles; however under lateral loading, the FRP piles exhibited larger deflections due to the inherent lower pile stiffness.

Most of the pile load tests and interface characterization studies using FRP materials have been conducted in sandy soils. There is a gap in knowledge regarding the behaviour of these materials, particularly frictional resistance under undrained conditions in clayey soils. This paper provides baseline information to compare the performance of FRP and steel piles in soft clays. This includes driving response, ultimate pile capacity under axial and lateral pile load tests and pile response under large lateral deflections. In addition, FRP material influence, comparing both carbon and glass fiber piles, fiber orientation and soil interaction are explored to determine optimal conditions for increased pile performance under field conditions. This was achieved by conducting a series of small scale pile load tests where model piles were driven in undisturbed clay samples collected in industrial sized steel drums. Following driving, axial and lateral static load tests were carried out. A description of the experimental setup and analysis of the results is presented in the sections below.

Soil sampling and properties

Undisturbed clay sampling

Pile load tests were carried out in undisturbed clay samples contained in industrial sized steel drums (876 mm in height and 597 mm in diameter). Soil sampling was conducted at a clay rich site in Navan, Ontario. The sampling was conducted as follows: (1) a thick section of clayey material was prepared by removing the top soil and leveling the surface ensuring that a clean profile of clay of at least 1.5 meters was present, (2) steel drums were placed upside down on the leveled soil surface, (3) using an excavator each steel drum was carefully embedded in the clay layer ensuring no cracking and minimal disturbance of the surrounding soil, (4) following embedment, the samples were carefully excavated and extracted, (5) the filled drums were sealed to prevent soil desiccation and to maintain the in situ conditions, (6) the soil containers were then shipped to the testing facility where the pile load tests were conducted. Fig. 1 illustrates the soil sampling procedure during the encasing of the steel drums.

Soil properties

The soil used for this study is a type of marine soft clay formed during the most recent ice age (cira 10,000 years ago) in the Ottawa River lowlands. This material, typically referred as Leda clay or Champlain Sea clay, is the result of glacial abrasion of the Canadian Shield resulting in a fine rock flour which was deposited at the bottom of the prehistoric saltwater Champlain Sea that flooded the region.

Fig. 1. Soil sample preparation for pile load tests.

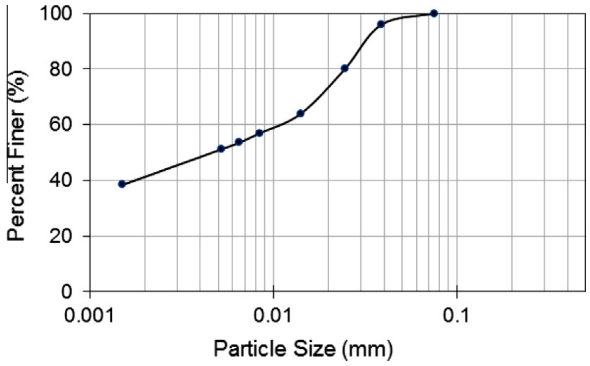

Fig. 2. Particle size distribution of Leda Clay.

The corresponding ASTM Soil characterization tests were carried out in order to determine the soil properties. Soil unit weight was measured at 15.3 kN/m^3 and it was classified as highly plastic clay (CH) according to the Unified Soil Classification System. Undisturbed undrained in situ shear strength was measured with a vane shear apparatus according to ASTM D2573 (2008) and was measured as 55 kPa throughout the steel drum depth profile. Atterberg limit tests were performed according to ASTM D4318 (2010) with measurements of a liquid limit and plasticity index of 51 and 23, respectively. Particle size distribution was determined as per ASTM D422 (2007) using a hydrometer test, and the results are illustrated in Fig. 2. The soil internal friction angle was determined using a direct shear box apparatus according to ASTM D6528 (2007) and was measured as 23.3°, under drained conditions at a rate of 0.05 mm/min. Table 1 summarizes the complete list of measured soil properties.

Model piles

A series of model FRP piles were manufactured with commercially available carbon and glass fabrics typically used for the reinforcement and retrofit of structural members. The raw material is in the form of fiber bundles woven into a coherent fabric in a uniaxial direction. Saturating the fabric in epoxy forms the FRP structure which can be molded into a number of different shapes and arrangements. The structural integrity of the cured fiber is provided primarily along the fiber direction. Manufacturing of the model FRP piles was carried out by using a steel mandrel around which the fiber fabric was fitted and allowed to cure following epoxy impregnation. Following a 48 h curing time, as per the manufacture's guidelines, the pile was extracted from the steel mandrel and cut to the required length. Pile dimensions were selected by carrying out a stress distribution analysis using commercially available geotechnical numerical software (Geostudio 2007). The goal of this analysis was to identify a pile length and diameter where boundary conditions of the soil confinement did not have a significant impact on the test results. The numerical analysis simulated small scale pile load testing using the geometry of the clay sample confined by the steel drum. Boundary conditions for the soil sample were simulated by applying displacement constrains along the outside model nodes representing the steel drum confinement of the soil sample. The pile was simulated as a steel member embedded in the soil with the appropriate geometric and elastic properties.

The model used linear-elastic properties for the soil and pile materials and Mohr–Coulomb material properties for the soil–pile interface. The analysis was carried out using axisymmetric behaviour under total and effective stress conditions utilizing interface parameters for steel under both drained and undrained conditions. The pile load test was simulated by applying 10 displacement increments of 1 mm in either the axial or lateral dimension at the pile head location for a total pile displacement of 10 mm. It was found through various iterations that a 700 mm pile length and a diameter of 55 mm would induce less than 10% of the applied stresses at the soil boundary, and accordingly these were the dimensions used for the model piles. The selected dimensions allow for 5 d (pile diameter) distance between the steel drum wall and the pile, providing adequate spacing to prevent influence from the boundary. Similar spacing of 3–5 d is typically used for preventing group pile effects for frictional piles (Tomlinson, 1994; Franke, 1984).

Five open-ended model piles were manufactured: 2 glass FRP piles (GFRP) and 3 carbon fiber (CFRP) piles. Pile wall thicknesses and diameter to thickness (d/t) ratios were maintained as constant as manufacturing permitted, and ranged from 3.6 to 4.15 mm in thickness and from 13.3 to 15.1 in d/t ratios (Table 2). These dimensions also allowed for a comparison to the control steel pile with a wall thickness of 3.45 and d/t of 14.2. For all piles, a total of 3 layers of fiber material was used which was the controlling parameter that dictated the wall thickness. Piles were manufactured with uniaxial alternating fiber direction which allowed for isolating the pile response to fiber orientation. In addition, the different fiber orientation and material fabrics cause changes in pile texture due to the differing wave patterns of the fiber fabric used. The GFRP piles were manufactured with three layers in either 0° or 90° orientations. Similarly the CFRP piles had the same arrangement, but with the addition of a third pile with two inner layers having fibers arranged along the pile axis (0°) and one outer layer with fibers perpendicular to the pile axis (90°). A control steel pile was prepared in order

Table 1
Soil properties for Leda clay.

ρ (Mg/m^3)	w (%)	LL (%)	PI (%)	w_{opt} (%)	$\rho_{d(max)}$ (Mg/m^3)	C_v (cm^2/s)	c_u (kPa)	ϕ (deg)	c (kPa)
1.53	49	51	23	30	1.41	1.40E−04	55	23.3	42.2

Notes: ρ, density; w, moisture content; w_{opt}, optimum moisture content; $\rho_{d(max)}$, maximum dry density; c_v, coefficient of consolidation; c_u, undrained shear strength; ϕ, internal friction angle; c, apparent cohesion.

Table 2
Model pile geometric properties.

Pile	Diameter d (mm)	Toe area (mm^2)	Length L (mm)	Thickness t (mm)	d/t	Fiber direction (°)	Epoxy to fiber content (%)
C-0	54.7	629.8	700	4.12	13.3	0	52.5
C-90	55.1	639.2	700	3.98	13.8	90	53.5
C-0/90	57.1	649.4	700	4.15	13.8	90/0	55
G-0	55.4	608.5	700	3.79	14.6	0	53.5
G-90	54.5	590.5	700	3.62	15.1	90	55.5
SP	49	493.7	700	3.45	14.2	N/A	N/A

C/G – denotes fiber material, number denotes fiber orientation.
SP – steel pile.

Table 3
Model pile material properties.

Pile	Ultimate tensile strength (MPa)	Tensile modulus (GPa)	Moment of Inertia (mm^4)	Initial flexural modulus (GPa)	Ultimate flexural modulus (GPa)	Initial stiffness (EI) (kN-m^2)	Stiffness at failure (EI) (kN-m^2)
C-0	986	98.5	2.04E+05	30	56.2	6.12	11.46
C-90	986	98.5	2.10E+05	–	–	–	–
C-0/90	986	98.5	2.29E+05	–	–	–	–
G-0	575	26.1	2.04E+05	25	32.6	5.10	6.8
G-90	575	26.1	1.91E+05	–	–	–	–
SP	400	200	1.29E+05	200	200	25.75	25.75

C/G – # denotes fiber material, number denotes fiber orientation.
SP – steel pile.

to compare the pile performance. Table 2 presents a summary of the geometric properties of the model piles tested. Additionally, a steel encasing mechanism at the pile head was used to apply axial and lateral loads to the piles and to prevent pile damage during driving.

Mechanical properties for the FRP composites, as reported by the manufacturer, are ultimate tensile strengths of 986 and 575 MPa and tensile modulus of 98.5 and 26.1 GPa for CFRP and GFRP, respectively. Additionally, test piles manufactured with fiber direction along the pile longitudinal were prepared and tested under three point bending according to ASTM D790 (2007) in order to characterize the pile flexural strength. Ultimate values for elastic modulus E, pile stiffness and other mechanical properties are listed in Table 3. It was observed however that pile stiffness EI varied non-linearly with the loading level. This non-linear behaviour is typical of FRP piles (Pando et al., 2006) and its implications regarding pile response will be discussed in subsequent sections. Finally, the epoxy/fiber ratio ranged between 50:50 and 45:55 as fiber saturation was observed in this range. This is typically the epoxy saturation ratio used for FRP piles and tubes (Fam and Rizkalla, 2002).

Experimental program

Test setup

A testing frame was assembled at Carleton University to apply monotonic axial and lateral loads for pile load tests. Schematics of the test assembly are shown in Fig. 3a. The horizontal reaction beam is assembled using two channel sections attached to the vertical columns. A steel plate was placed across the channel section which served as a reaction platform allowing for the application of compressive loads. Axial load was applied using a hydraulic jack coupled to a steel rod connected to the pile head which runs vertically aligned with the pile axis. Force measurement was carried out using a load cell placed at the jack – pile head connection ensuring proper alignment. Lateral loading was applied using a lateral bracing system connected to the vertical reaction columns. A steel rod was used to attach the pile head to the hydraulic jack which was resting horizontally against the reaction lateral brace. The steel rod was attached to the pile head by means of a U-shaped brace around the pile head which was connected to the steel rod by an end-bearing joint allowing for horizontal self-alignment as load was applied. A schematic top view for the lateral loading system is illustrated in Fig. 3b.

All model piles were open-ended and driven to an embedment depth of 700 mm. Driving records and rates of penetration for the different piles are shown and discussed in the following sections. The load tests were carried out immediately following driving to prevent time-dependent pile set-up effects. Axial and lateral resistance was measured using a load cell connected to a data logging station, while axial and lateral displacement at the pile head was recorded with an LVDT device connected to the reference beams. All the data was collected by an automated data logging station with calibrated recording software. Fig. 4a shows the experimental assembly before driving of the pile. Fig. 4b illustrates the assembly of the pile head system and the vertical steel rod undergoing axial loading and Fig. 4c shows the setup undergoing lateral loading.

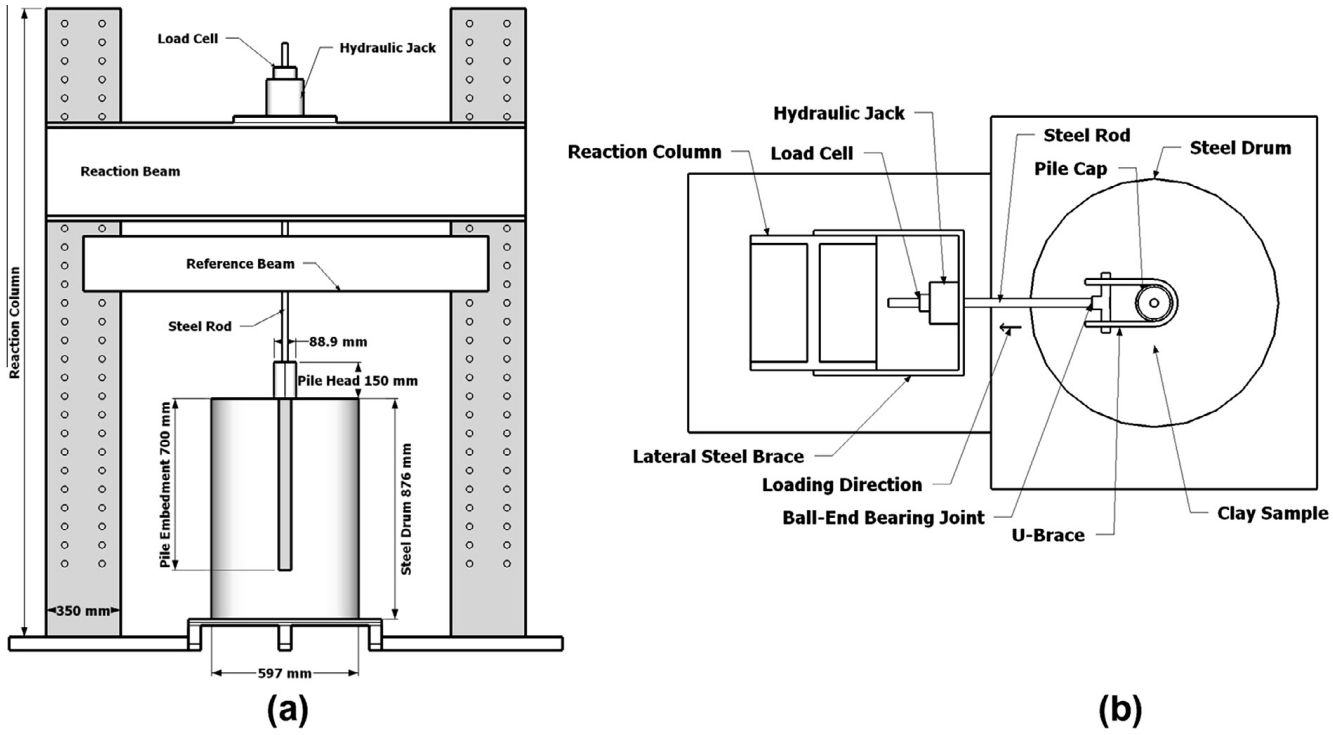

Fig. 3. (a) Experimental setup and (b) lateral loading schematics.

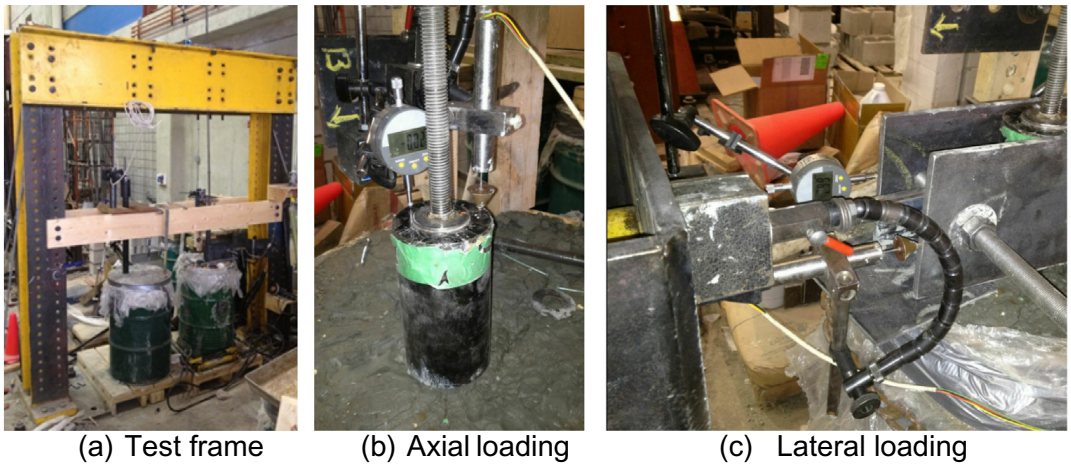

Fig. 4. Experimental assembly for axial and lateral load tests.

Pile driving

Pile driving was carried out using a pulley and drop hammer setup. The drop hammer weight and drop distance were kept constant throughout the test at 8.8 kg and 150 mm, respectively. The impact energy was approximately 15 joules per blow. Driving was carried out at approximately 10–15 blows per minute with a rate of penetration ranging from 10 mm/blow at shallow depths to as low as 2 mm/blow when reaching the target depth. Fig. 5a shows the cumulative blow count vs. penetration depth ratio d/z (diameter over depth) and Fig. 5b shows the rate of penetration vs. the depth ratio. It is evident there are two main regions where there is a marked increase in driving resistance at approximately 4 diameters of penetration possibly following the penetration of the top few inches of disturbed soil material due to sampling and pile driving. In addition, all FRP piles presented similar penetration ratios, while the steel pile penetration ratio was up to 25% lower at lower driving depths.

Test procedure

Static compressive pile load tests

Compressive pile load tests were carried out following a modified method based on ASTM D1143 (2007). The pile head mechanism was used to connect a steel rod to the hydraulic jack and the reaction frame allowing for the

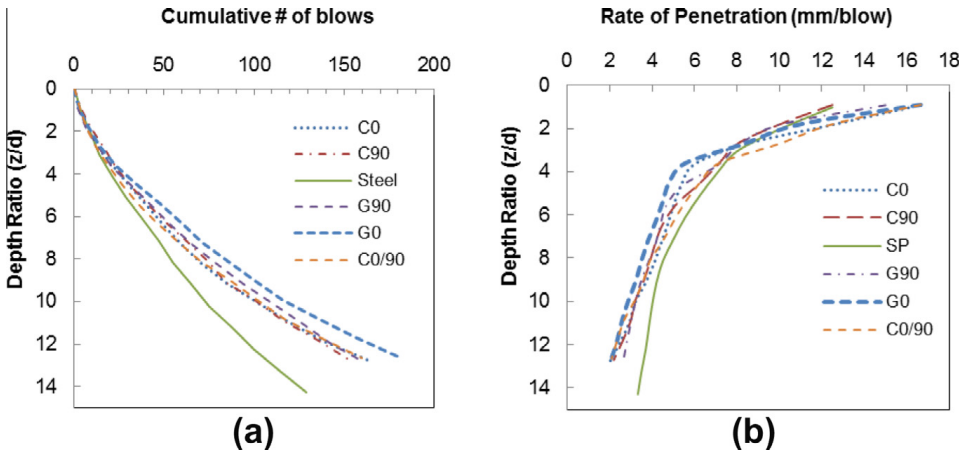

Fig. 5. (a) Cumulative # of blows vs depth ratio; (b) rate of penetration vs depth ratio.

application of compressive loads. The loading procedure was designed to bring the pile to failure by applying incremental loading at 100 s intervals, allowing for interface forces to reach equilibrium. The failure criteria used to determine ultimate pile capacity was the pile resistance at a pile head displacement of 10% pile diameter as suggested by De Nicola and Randolph (1999). For all tests, the number of loading cycles required to reach the mentioned failure criteria ranged from 14 to 17. Pile unloading was carried out in 4 steps and pile rebound was measured.

Static lateral load tests

Following axial compression testing, a lateral pile load test was carried out according to a modified procedure based on ASTM D3966 (2007). The test was carried out by applying load increments at 100 s intervals. Unlike compressive tests, lateral load tests did not reach the defined failure behaviour. Typically, the design criteria for lateral pile capacity are based on limiting pile head deflection. The failure criteria used for determining ultimate pile capacity was the capacity measured 6.25 mm of pile head displacement as suggested by Prakash and Sharma (1990), however the loading test was continued until approximately 0.20 was reached for the displacement ratio (pile head movement/pile diameter) to observe pile behaviour at large lateral deflections. The average number of cycles required to reach the failure criteria ranged from 20 to 25, at which unloading was carried out in 4–5 cycles and pile rebound was measured.

Results and discussion

Pile axial compression capacity

Pile load test results are summarized in Fig. 6 where axial load capacity is plotted against vertical pile head movement. Ultimate pile capacity was defined as the load corresponding to a pile head displacement equal to 10% of the pile diameter (De Nicola and Randolph, 1999). At this level of displacement (5.5 mm), pile capacity was observed to remain approximately constant with each additional loading cycle. Table 4 summarizes the pile capacity for all FRP and steel piles. In all cases, ultimate capacity

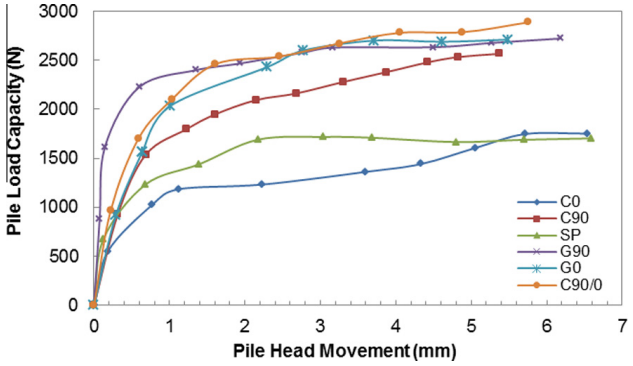

Fig. 6. Pile resistance vs pile head movement.

for the FRP model piles was 25–40% higher than the steel pile with the exception of the C0 pile which was on par with the steel pile ultimate capacity. The loading response of all piles was similar, with a rapid linear increase in pile resistance at very low pile head displacements, attributed to ultimate shaft frictional capacity being mobilized followed by a hardening region until ultimate capacity is reached at approximately 5.0–5.5 mm of displacement.

Pile frictional resistance was observed to engage at very low displacements ranging from 0.08 mm to 0.16 mm corresponding to 0.15–0.30% of pile diameter. Pile G90 presented the fastest rate of capacity increase while the steel and C0 piles presented the most gradual increases. The rapid change in slope of the load–displacement curve after the early portion of loading can be attributed to frictional failure of the soil surrounding the pile shaft. Further pile movement engages soil at the pile toe providing a very gradual increase of capacity due to the open-ended nature of the pile geometry.

Based on the pile load tests results shown above, it is evident that the FRP piles tested present a significant improvement over traditional steel piles in terms of their axial capacity performance in soft clays. Full scale pile load tests are required to verify pile driving performance, structural resistance, and long term effects such as creep and weather resistance. As FRPs gain a better established track record and increased industry use, economies of scale will

Table 4
Axial compressive capacities of FRP and steel piles.

Pile	Compressive capacity (N)	Shaft resistance (N)	Estimated shaft resistance (N)	Toe resistance (N)	Shaft resistance ratio (%)
C-0	1670	1330	1453	340	79.6
C-90	2567	2220	2041	345	86.4
C-0/90	2786	2436	N/A	350	89.8
G-0	2711	2383	2255	328	89.9
G-90	2722	2404	2194	318	88.3
SP	1710	1440	1546	266	84.2

bring prices down to match that of steel piling. Furthermore, GFRP piles exhibited some of the largest pile resistances tested while material costs are half of the CFRP piles.

Pile shaft resistance

Pile capacity of open-ended piles in cohesive soils is developed primarily in the form of soil–pile adhesion, also referred to as pile shaft resistance, in undrained conditions. Various authors (Poulos and Davis, 1980; Fleming, 1992) and design guidelines such as the CFEM (Canadian geotechnical society, 2007) estimate the pile bearing capacity as a function of pile geometry (length and diameter) and soil–pile interface resistance. The shaft resistance (Q_s) is typically estimated from the following equation:

$$Q_s = CLq_s \tag{1}$$

where C is pile circumference, L is pile embedment and q_s is the average shear strength, also known as unit shaft resistance, along the soil–pile contact area. Furthermore the average shear strength q_s can be expressed in terms of the soil undrained shear strength (c_u) and an empirical reduction factor, α, accounting for pile–soil adhesion which is typically correlated to c_u. q_s is estimated by the following equation:

$$q_s = \alpha c_u \tag{2}$$

Bearing capacity of open-ended driven piles in clay is mainly provided by shaft resistance, with a minimal contribution from toe bearing resistance. Toe bearing resistance has been estimated and removed from the total pile capacity in order to isolate the shaft resistance. Toe capacity (Q_b) was calculated according to the following expression:

$$Q_b = N_c c_u A_b \tag{3}$$

where N_c is a bearing capacity factor, typically 9 for pile diameter under 0.5 m as suggested by CFEM (Canadian geotechnical society, 2007). c_u is the soil undrained shear strength, and A_b is the pile toe contact area. On average, the calculated toe bearing capacity was estimated to be approximately 10–15% that of the measured pile resistance for all model piles.

The average unit shaft resistance, q_s, was estimated from the measured pile capacities by dividing the load transferred to the soil between the pile head and toe by the surface area of the pile, as follows:

$$q_s = \frac{Q - Q_b}{CL} \tag{4}$$

where Q is the measured pile capacity, Q_b is the toe resistance, C is pile circumference, and L is pile embedment. Fig. 7 illustrates the comparison of average unit shaft resistance plotted against displacement ratio (pile head movement/average pile diameter) for all piles. In all cases failure was estimated to occur at a displacement ratio of approximately 0.1. It is clear that both glass fiber G0, G90 and the carbon C90/0 model piles reached the highest shaft resistance at approximately 20 kPa compared to steel pile at 13.5 kPa for an overall improvement of up to a 30% increase. In contrast, pile C0 presented an overall decrease in shaft resistance of up to 15% at pile failure. The higher shaft resistances of FRP piles are attributed to their surface roughness compared to the steel pile. Pile surface texture plays a significant role in the increased shaft resistance because grooves and textures in the pile fabric create increased contact area between the soil and pile. Similar behaviour was observed when different FRP fabrics were sheared against soft clay in a direct shear box (Giraldo and Rayhani, 2013). Large scale pile load tests are needed to corroborate these results.

The corresponding α-coefficient for each pile load test was estimated using Eq. (2). The α value for piles G0, G90 and C90/0 was 0.36, for pile C90 it was 0.33 and for pile C0 it was the lowest value at 0.21. In addition, the control steel pile was measured at α of 0.25. The calculated values are, in general, lower than the typical estimates reported in the literature for clays of similar undrained shear strength (Poulos and Davis, 1980; Fleming, 1992; Canadian geotechnical society, 2007). Additionally, shaft resistances estimated based on undrained interface parameters obtained from interface shear strength values carried out by Giraldo and Rayhani (2013) are presented in Table 4. The results indicate a good agreement with the measured shaft

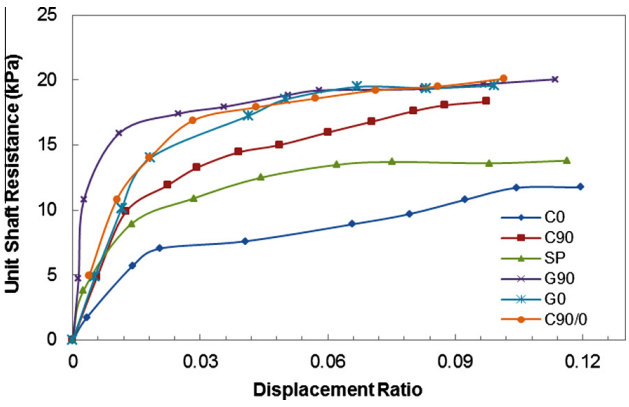

Fig. 7. Average unit shaft resistance of FRP and steel piles.

resistance values from pile load testing with the largest discrepancy of 8% between the estimated and measured values.

Effect of fiber orientation on pile capacity

Fiber orientation was investigated in order to characterize its influence on pile capacity. Since pile surface texture was dictated by the weave pattern of the fiber fabric used to manufacture the piles, changing the direction of the fiber significantly modified the pile texture in contact with the soil. More importantly, GFRP piles had a distinct interwoven fiber bundling pattern which gave the pile surface protruding ridges and valleys with approximately 0.5 mm peak to valley distances that changed direction depending on pile manufacturing. In contrast, for CFRP piles the texture was streamlined with less pronounced ridges. However CFRP oriented at 0° allowed for streamlined groves along the pile axis which is suspected to allow the unobstructed sliding of clay, leading to the lower pile capacity measured. Fig. 8 illustrates the frictional performance of three CFRP model piles each with fibers parallel and perpendicular to each other against pile displacement ratio. The third pile C90/0 has the outer surface with fibers oriented at 90° with the objective of providing better soil–pile resistance, while the inner fibers provide the pile with structural integrity. This combination is shown to present the best results in terms of shaft resistance for the CFRP piles with over a 35% increase of the C90/0 pile at pile failure. Further testing and stringent manufacturing quality control to ensure pile surface texture repeatability are needed to characterize the influence of pile texture and fiber orientation in a consistent manner. With respect to GFRP piles, both piles reached similar frictional capacity at failure suggesting that the pronounced texture of the pile surface interacting with the soil is independent of groove orientation, suggesting that the increased surface area available at the soil–pile interface was responsible for the increased shaft resistance. However, it was observed that pile G90 experienced shaft resistance mobilization at lower displacement ratios than pile G0. No GFRP pile with combined fiber orientation was produced since pile G90 was observed to have the sufficient structural integrity required to withstand testing at the low axial loads used in this small scale study. Further analysis of optimal fiber orientation is needed in order to establish optimal structural integrity of the pile in order to avoid structural failure. In both cases, (GFRP and CFRP) the optimal outer surface fiber orientation was 90° with pile shaft resistance. The CFRP piles showed a higher sensitivity to fiber orientation than GFRP piles. Inner layers of FRP should be arranged in a fashion to increase pile structural integrity. Full scale pile load tests are needed in order to explore the pile behaviour under working loads.

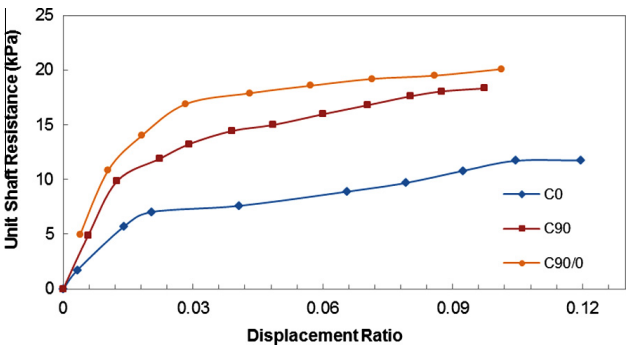

Fig. 8. Comparison of CFRP pile performance on based on fiber orientation.

Effect of FRP material selection on pile capacity

Selection of pile material has an important role in two key aspects of pile performance: pile structural integrity and geotechnical response. Structural integrity is directly linked to the mechanical material properties such as elastic modulus and yield strength, whereas pile geotechnical performance is strongly influenced by the pile surface texture which is dictated by the weaving of the fabric. Based on the results of this study, the GFRP piles tested in both 90° and 0° orientations presented a significant improvement over steel, while fiber orientation strongly influenced pile resistance for CFRP piles, leading to significantly lower pile capacity in the 0° fiber direction. Fiber weaving and texture had a significant effect and the GFRP pile specimens showed protruding ridges due to the fabric weaving manufacturing process which is suspected to allow for increased soil–pile surface area or a better soil–pile interlocking mechanism. From a geotechnical point of view, the surface texture produced by the GFRP material yields a better performance than the CFRP fabric. To date most studies regarding structural response of hollow and concrete filled FRP tubes have been conducted with GFRP fibers since the high cost of CFRP materials has not made the production of CFRP piles feasible for large scale use. However, studies on the structural response of GFRP piles have shown that hollow GFRP piles are susceptible to buckling (Frost and Han, 1999). In addition, long term deformations such as creep can be significant issues for FRP piles due to material anisotropy, lower moduli and higher shear to elastic moduli ratios compared to steel. Approaches to increase structural performance of FRP piles include the partial or total infilling of the hollow void with concrete in order to take advantage of the confining effect of the concrete by the FRP shell (Fam and RizKalla, 2001a,b).

Pile lateral capacity

Pile lateral capacity is typically determined by estimating the ultimate lateral failure load divided by a safety factor or by estimating the allowable lateral load corresponding to acceptable pile deflections based on various design criteria. The failure load, based on the static lateral loading test, was taken as the pile resistance measured at 6.25 mm (0.1 displacement ratio) of lateral pile head movement (Prakash and Sharma, 1990). However, the loading test was carried out until a pile head movement of 20% pile diameter (displacement ratio) occurred to observe the behaviour of the model piles under large deformations. Piles were assumed to behave as short free – head piles as the L/d ratio for all the piles ranged from 13.5 to 12.7. Typically, short pile behaviour is expected

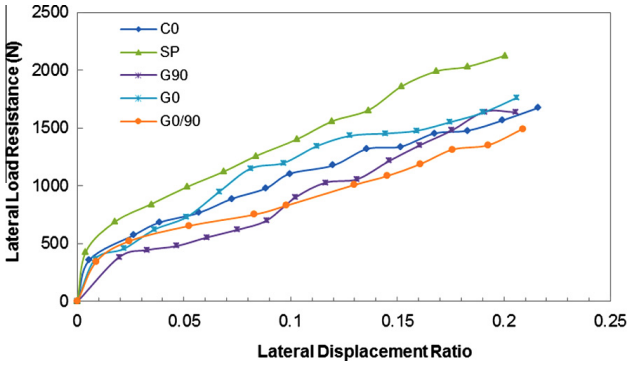

Fig. 9. Lateral pile resistance vs pile displacement ratio.

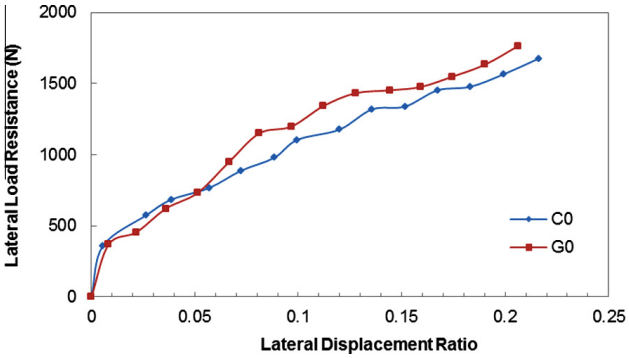

Fig. 10. Effect of FRP material selection on lateral pile capacity.

for pile with L/d ratios of 10–12 (Tomlinson, 1994). In addition, the maximum applied lateral load was lower than the load at failure under 3-point bending tests for the tested FRP piles illustrating that flexural material failure is not the controlling parameter for the tested piles.

Fig. 9 illustrates the results for 5 pile load tests showing lateral resistance and pile displacement ratio (lateral movement divided by pile diameter). Pile C90 failed structurally when subjected to lateral loads due to the lack of longitudinal fiber reinforcement; hence the results are not included in this analysis. In all cases the load–displacement behaviour exhibits two approximately linear sections. At low lateral displacement ratios of 0.01–0.02, loading response is characterized by a rapid increase in lateral resistance, followed by an approximately linear trend with a less pronounced slope. The steel pile presented an increase in lateral resistance up to 28% higher at failure compared to the FRP piles. Similar behaviour was reported by Sakr et al. (2004) in scale piles tested in a pressure chamber filled with sand. The lower pile response was mainly attributed to the lower flexural stiffness of the FRP piles (E_pI_p). In addition Pando et al. (2006) discussed the susceptibility of FRP piles, especially hollow FRP piles to increased lateral deflections due to shear deformation effects caused by high ratios of elastic to shear modulus. Table 5 shows a summary of the lateral capacity for the different piles and their corresponding flexural stiffness (EI) estimated from 3 point loading tests. It was observed based on these flexure tests that the piles at peak lateral displacement ratios of 0.2 were only approximately under 20–30% of their ultimate flexural capacity, and well below structural failure. Full scale load tests are needed to explore FRP pile behaviour under working load conditions.

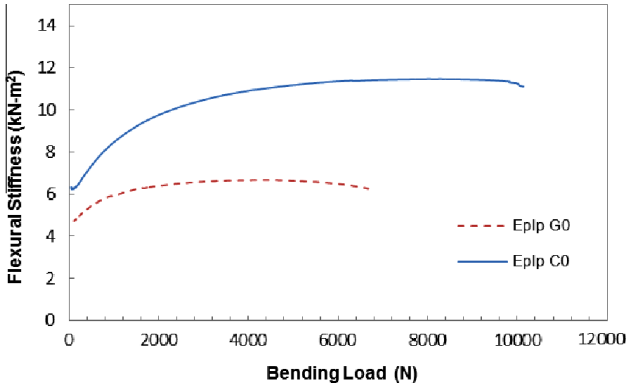

Fig. 11. Comparison of pile flexural stiffness under 3-point bending.

Effect of pile material on lateral capacity

Pile response under lateral loading is typically controlled by soil response, pile stiffness and soil–pile interface interaction. For this research program, lateral response is mainly controlled by the model pile structural properties such as the piles flexural stiffness E_pI_p since soil conditions and pile geometry is approximately equal for all cases. Fig. 10 shows the lateral response of piles C0 and G0 illustrating no significant difference in pile behaviour, with pile G0 showing only a 5% increase in pile capacity. Fig. 11 illustrates the results for flexural stiffness vs loading level carried out under 3-point bending. It is shown that the pile behaviour is highly non-linear at low loading levels reaching a plateau after approximately 30% of failure load. The FRP model piles under lateral load at 0.2 displacement ratio face a load of approximately 2000 N at the pile head corresponding to approximately 20% of the failure loading under 3-point

Table 5
Lateral capacity and properties of FRP and steel piles.

Pile	Lateral capacity at 6.25 mm (N)	Pile stiffness (E_pI_p) at 2000 N load (kN-m^2)	Pile stiffness (E_pI_p) at failure (kN-m^2)	Lateral resistance ratio to steel
C-0	880	6.4	6.8	80.0
C-90	N/A	N/M[a]	N/M[a]	86.4
C-0/90	650	N/M[a]	N/M[a]	59.0
G-0	950	9.7	11.4	86.6
G-90	580	N/M[a]	N/M[a]	52.0
SP	1100	25.75[a]	25.75[b]	

[a] N/M – not measured under 3-point bending.
[b] Calculated based on 200 GPa elastic modulus.

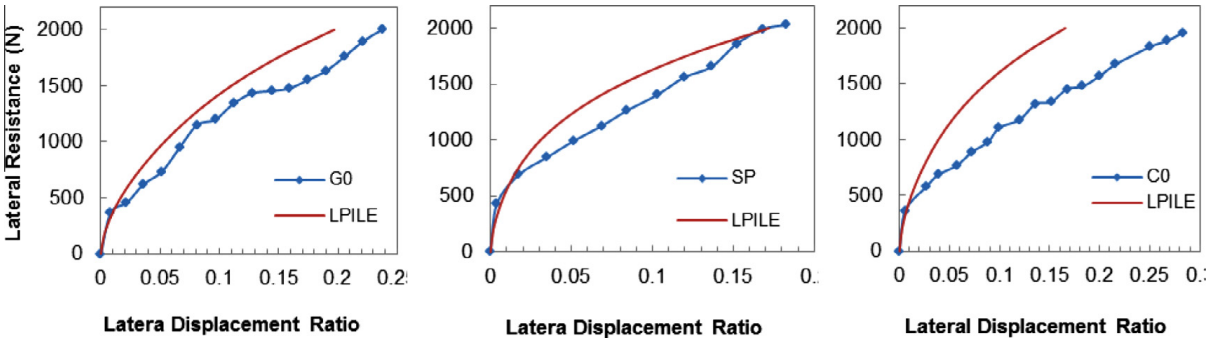

Fig. 12. Measured lateral capacities vs LPILE analyses for FRP and steel piles (G0; glass FRP, SP: steel and C0: Carbone FRP).

bending. This indicates that the pile flexural stiffness for piles undergoing lateral loading is in the range of 6.7–9.3 kN-m^2 for G0 and C90, correspondingly. Although 3-point bending does not accurately represent the bending moments applied to a pile under lateral loading, these values give a basic understanding of why these piles experience higher deflections than their steel counterpart. Based on this study it is difficult to identify which material performs optimally under lateral loading since the pile stiffness behaves non-linearly and the soil yielded before pile failure occurred. It was obvious however, that both FRP piles present a significantly softer response than steel piles.

Comparison to analytical lateral capacity estimates

Lateral pile capacity is usually carried out by estimating ultimate pile capacity through methods considering lateral earth pressure theory such as the Brinch Hansen Method (Brinch Hansen, 1961) or Broms' theory (Broms, 1964) or by estimating acceptable deflections at a working load. Estimating pile deflections typically uses the elastic continuum solution and modulus of subgrade reaction approaches such as *p–y* curves to calculate pile deflections at a given loading condition. A numerical analysis was carried out using the *p–y* method to compare typical design approaches applied to the response of the FRP piles. *P–y* curves are typically developed for specific soil types and pile geometries (Prakash and Sharma, 1990). The family of *p–y* curves used for this study was based on method proposed by Matlock (1970) which was developed for soft to medium clays. The analysis was carried out using the commercially available software typically used for design estimates LPILE (Ensoft Inc., 2013) which allows the input of pile properties, boundary and loading conditions and the built in *p–y* curves.

The simulation used the same laboratory parameters with the same thickness for the uniform clay layer, pile dimensions and geometric properties and stiffness response based on results measured from the 3-point bending tests on piles at a similar loading level as the lateral loading test. The soil was modeled as an elasto-plastic medium with Mohr–Coulomb constitutive behaviour, while the pile was modeled as a linear elastic element. Loading was applied in 10 increments until a total 2000 N lateral loading was reached. Measurements of pile head deflection at the different loading intervals were then compared to the lateral test results. It is important to note that the numerical simulation using LPILE does not take into account the steel drum sample confinement and assumes an infinitely long soil layer in the horizontal direction. This effect can be one of the reasons for some of the discrepancies observed between the measured and estimated lateral deflections of some of the tested piles. The results comparing the behaviour of the steel pile, C0 and G0 piles are show in Fig. 12.

Similar resistance–displacement behaviour was found between the steel pile and LPILE results with similar pile head displacements throughout the loading procedure. Although the GFRP pile presented a reasonable agreement with LPILE results, the CFRP pile presented a discrepancy of up to 35% pile head deflection difference. This could be attributed to non-linear material deformation of the CFRP pile not accounted in the LPILE model as the element was modelled as a linear-elastic pipe with constant EI. A more elaborate numerical analysis accounting for FRP non-linear deformation is probably needed to accurately model the FRP piles behaviour in LPILE. Pando et al. (2006) carried out a similar analysis for concrete filled FRP piles in sand with a similar approach using LPILE software where they found good agreement between the modelled and measured pile deflections with the implementation of a non-linear EI in their modelling. Full scale tests using instrumented piles are required to accurately measure pile deformations along the shaft in order to characterize the pile stiffness non-linearity, and better predict pile deflections under working loads.

Conclusions

A series of small scale static pile load tests in laboratory was carried out to characterize the performance of open-ended FRP piles in clayey soils. The major findings of this research programme are summarized below:

- Compressive ultimate pile resistance of the model FRP piles was up to 40% higher than the control steel pile. Similarly skin frictional resistance of the FRP piles was measured to be up to 30% higher with both CFRP and GFRP.
- GFRP piles presented a highly textured surface due to the raw fiber weaving pattern with both directions 0° and 90° showing significant protrusions. In contrast the CFRP pile presented a less pronounced surface texture with the 90° orientation showing an increased profile.

- FRP pile texture and waviness appeared to have a significant influence on pile performance with CFRP piles ranging from just 5% capacity increase to up to 40% by changing pile fiber direction and surface texture. In contrast, the GFRP piles presented virtually the same ultimate capacity at a 40% increase over steel despite changes in fiber orientation.
- Lateral loading of the piles showed that the lower stiffness of the FRP piles leads to increased pile head deflections at similar loading levels compared to the baseline steel pile. These results agree with similar tests carried out in sandy soils
- The modelling of the steel, C0, and G0 piles under lateral loading was carried out using LPILE numerical software to compare common design methods to the performance of FRP piles. The steel pile presented comparable results while both FRP piles presented higher pile head deflections compared to the numerical simulation. In the analysis, linear elastic properties were provided as input as is common practice in pile design. FRP piles however can present non-linear behaviour under loading which can lead to the measured discrepancies.

The results of this study highlight the viability of FRP piles in soft clays as an alternative to traditional steel piles. Axial compressive capacity was measured to be up to 40% higher than steel, where pile surface and texture appeared to have a significant influence on pile performance. Lateral response of FRP piles showed higher deflections at similar loading levels compared to steel. These results are in line with similar research conducted in sands and are primarily due to the lower elastic modulus and stiffness compared to steel and prestressed concrete.

Acknowledgements

This study was financially supported by the Natural Sciences and Engineering Research Council of Canada (NSERC). The authors are also grateful to their industrial partner, Fyfe Co., for providing FRP samples for testing; however, the views expressed herein are those of the writers and not necessarily those of our partner.

References

Ashford SA, Jakrapiyanun W. Drivability of glass FRP composite piling. J Compos Constr 2001;5:58–60.
ASTM D1143. Standard test methods for deep foundations under static axial compressive load. West Conshohocken, PA: ASTM International; 2007. http://dx.doi.org/10.1520/D1143_D1143M-07E01.
ASTM D2573. Standard test method for field vane shear test in cohesive soil, west. West Conshohocken, PA: ASTM International; 2008. http://dx.doi.org/10.1520/D2573-08.
ASTM D3966. Standard test methods for deep foundations under lateral load. West Conshohocken, PA: ASTM International; 2007. http://dx.doi.org/10.1520/D3966-07.
ASTM D422. Standard test method for particle-size analysis of soils. West Conshohocken, PA: ASTM International; 2007. http://dx.doi.org/10.1520/D0422-63R07.
ASTM D4318. Standard test methods for liquid limit, plastic limit, and plasticity index of soils. West Conshohocken, PA: ASTM International; 2010. http://dx.doi.org/10.1520/D4318-10.
ASTM D6528. Standard test method for consolidated undrained direct simple shear testing of cohesive soils. West Conshohocken, PA: ASTM International; 2007.
ASTM D790. Standard test methods for flexural properties of polymer matrix composite. West Conshohocken, PA: ASTM International; 2007. http://dx.doi.org/10.1520/D1143_D1143M-07E01.
Brinch Hansen J. The ultimate resistance of rigid piles against transversal forces. 1961, Geoteknisk Institut, Copenhagen, Bull No. 12.
Broms BB. Lateral resistance of piles in cohesive soils. J Soil Mech Found Div., ASCE 1964;90(2):27–67.
Canadian geotechnical society. Canadian geotechnical engineering manual. 4th ed. Richmond: BC, BiTech Publishers Ltd.; 2007.
De Nicola A, Randolph MF. Centrifuge modelling of pipe piles in sand under axial loads. Géotechnique 1999;49(3):295–318.
Ensoft Inc. LPILE v. 6. 2013, [Online] available at: http://www.ensoftinc.com/ [Cited 23 07 2013].
Fam AZ, RizKalla SH. Behavior of axially loaded concrete-filled circular fiber-reinforced polymer tubes. ACI Struct J 2001a;98(3):280–9.
Fam AZ, Rizkall SH. Confinement model for axially loaded concrete confined by FRP tubes. ACI Struct J 2001b;98(4):251–61.
Fam AZ, Rizkalla SH. Flexural behaviour of concrete-filled fiber-reinforced polymer circular tubes. J Compos Constr 2002;6(2):123–32.
Fleming WG. Piling engineering. New York: Halsted Press; 1992.
Franke E. Group action between vertical piles under horizontal loads. Proceedings of the International Geotechnical Seminar on Deep Foundations on Bored and Auger Piles, Ghent, Belgium, 1984, pp. 83–93.
Frost JD, Han J. Behaviour of interfaces between fiber-reinforced polymers and sands. J Geotech Environ Eng 1999;125(8):633–40.
Geostudio 2007. A software package for geotechnical analysis.
Giraldo J, Rayhani MT. Influence of fiber-reinforced polymers on pile–soil interface strength in clays. Adv Civil Eng Mater 2013;2(1). ID ACEM20120043.
Guades E, Aravinthan T, Islam M, Manalo A. A review on the driving performance of FRP composite piles. Compos Struct 2012;94:932–1942.
Han J, Frost JD. Load–deflection response of transversely isotropic piles under lateral loads. Int J Numer Anal Meth Geomech 2000;24:509–29.
Iskander MG, Hassan M. State of the practice review in composite piling. J Compos Constr 1988;2:116–20.
Iskander MG, Hanna S, Stachula A. Driveability of FRP composite piling. J Geotech Geoenviron Eng 2001;127:169–76.
Matlock H. Correlation for design of laterally loaded piles in soft clay. Proceedings Offshore Technology Conference, 1970, paper OTC 1204.
Mirmiran A, Shahawy M, El Khoury C, Naguib W. Large beam-column tests on concrete-filled composite tubes. ACI Struct J 2000;97:268–76.
O'Rourke TD, Druschel SJ, Netravali AN. Shear strength characteristics of sand–polymer interfaces. J Geotech Eng 1990;116(3):451–69.
Pando AM, Flitz MG, Dove JE, Hoppe EJ. Interface shear tests on FRP composite piles. International Deep Foundations Congress. Orlando, FL: ASCE; 2002. pp. 1486–1500.
Pando AM, Ealy CD, Flitz MG, Lesko JJ, Hoppe EJ. A laboratory and field study of composite piles for bridge substructures. McLean, VA: Federal Highway Administration; 2006. Report No. FHWA-HRT-04-043.
Poulos HG, Davis EH. Pile foundation analysis and design. New York: John Wiley and Sons Inc.; 1980.
Prakash S, Sharma HD. Pile foundations in engineering practice. New York: John Wiley and Sons Inc.; 1990.
Sakr M, Elnaggar H, Nehdi M. Novel toe driving for thin-walled piles and performance of fiber-reinforced polymer (FRP) pile segments. Can Geotech J 2004;41:313–25.
Tomlinson M. Pile design and construction practice. 4th Ed. New York: E & FN Spon, an Imprint of Chapman & Hall; 1994.